# Proposal of Automatic Power Plug Insertion Control for Electric Vehicle with In-Wheel-Motors

Daiki Kusuyama, Tomoki Emmei, Hiroshi Fujimoto, Yoichi Hori
The University of Tokyo
5-1-5, Kashiwanoha, Kashiwa, Chiba, 227-8561, Japan
kusuyama@ieee.org, enmei.tomoki14@ae.k.u-tokyo.ac.jp, fujimoto@k.u-tokyo.ac.jp, hori@k.u-tokyo.ac.jp

***Abstract*—Electric Vehicles (EVs) have attracted significant attention, and users are enjoying increasing opportunities to recharge EVs by themselves in parking lots. However, the task of power plug insertion is a heavy burden for users particularly with weak power, because the power supply cables for EVs, carrying a large amount of electricity, are heavy and thick. In this paper, we propose a control method of automatic power plug insertion by applying the reaction force/moment control. The reaction force/moment is estimated with a driving force observer and a yaw-moment observer. These estimates are fed back to regulate the reaction force to the desired value and the reaction moment from the power plug to 0. Simulation and experimental results show that the proposed method can accurately estimate the reaction force/moment and control them appropriately. These results demonstrate that proposed method can achieve automatic power plug insertion.**

***Index Terms*—Electric vehicle, in-wheel-motor, non-holonomic system, force control, force estimation, peg-in-hole**

## I. Introduction

In recent years, electric vehicles (EVs) have attracted significant attention due to the growing awareness of air pollution and the exhaustion of fossil fuels. EVs also have the following advantages in terms of motion performance: torque response is about two orders of magnitude faster than that of gasoline-powered vehicles; advanced control and estimation can be realized because output torque can be easily measured; motors can be distributed [1].

Distributing motors makes In-Wheel-Motor (IWM) type EV possible: each driving motor can be placed inside each wheel. With IWM, information from each wheel can be utilized, and each IWM can be driven independently. By taking advantage of this, numerous control methods have been proposed, e.g., anti-slip control, collision avoidance for passenger safety, vibration suppression control for ride comfort or range extension autonomous driving [2]–[4].

The cruising range problem, the most significant disadvantage of EVs, has already been overcome. Unlike gasoline-powered vehicles, EVs have a variety of options for where and how to charge them because they do not need to refill liquid fuel. One such option is to power an EV while driving. A large number of works have been conducted on it, and wireless power transfer (WPT) technology while driving [5] and contact charging technology while driving [6] have been established.

On the other hand, in case of charging EVs while parking, users have a more excellent opportunity to recharge EVs by themselves in parking lots such as homes or shopping malls, because EV charging stations can be installed anywhere where electricity is available. However, power supply cables for EVs are heavy and thick because they need to carry a large amount of electric power. Thus, inserting a power plug is a heavy burden for users, particularly with low power. Since charging stations are often installed outdoors, it is necessary to insert the power supply cable contaminated with mud while getting wet. These impede the convenience of EVs as a means of transportation in rainy weather.

(a) Overall view of the vehicle. (b) Enlarged view of the power plug and socket.

Fig. 1. Experimental vehicle with IWM: FPEV-2 Kanon.

Therefore, WPT has been widely studied all over the world, and our research group established the technology to supply power by WPT [5], [7]. However, it will take some time before WPT systems become common because of some problems such as the risk of circuit failure caused by an eddy current when there are metal particles between the transmission coil and receiving coil, and the high cost of installing additional equipment on both the transmission side and the vehicle body side.

In this study, we propose the use of autonomous driving technology that allows EVs to insert the power plug by themselves and to recharge by wire using only existing equipment. This method overcomes the disadvantage of forcing users to insert power plugs while at the same time taking advantage of the fact that power can be supplied efficiently without additional equipment, which is the main benefit of wired power supply. The following three tasks are necessary to achieve automatic power plug insertion: 1) to generate a parking route in which a power plug can be inserted, 2) to move on to the

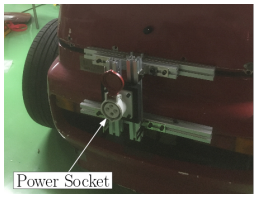


(a) Power socket attatched to the experimental vehicle.


(b) Force/moment sensor used to measure the actual reaction force/torque.

Fig. 2. Equipments used in the experiment.

given path and let the power socket contact, and 3) to apply the desired force for insertion. Of these tasks, path generation and path following have been achieved in previous researches [8], [9]. Thus, we describe a method of applying force control to EVs, using only the driving force of EVs to generate the desired force to insert a power plug into a power socket.

In past researches of vehicle motion control, position control for automatic parking or path following and velocity control for cruise control or anti-slip control is often used. Most of the force related control methods are disturbance suppression control such as yaw moment control or braking force control such as Anti-lock Braking Systems. However, previous researches do not address applying force control to EV body, except for [10].

On the other hand, there are many studies on force control of robot which interact with environments [11]–[14]. [15] proposed impedance control in which adjusts imaginary impedance between the robot and the environment. [16], [17] developed hybrid control in which the endpoint of the robot follows a command orbit exerting a desired force on the environment. However, these methods cannot be directly applied to vehicles which are underactuated and non-holonomic systems since most of these researches address systems with a sufficient degree of freedom (DOF) such as a 6-DOF manipulator.

Therefore, we propose applying force control to IWM-EVs without any additional sensors to achieve automatic power plug insertion considering non-holonomic constraints as a prerequisite. The experimental condition are described in section Ⅱ, The proposed method of the estimator and the controller are introduced in section Ⅲ and in section Ⅳ, simulation results and experimental results are shown. Finally, the conclusion is in section V.

## II. Electric Vehicle with In-Wheel-Motors

### A. Experimental setup

Fig. 1 shows an experimental setup for this research. The vehicle, FPEV-2 Kanon, has four IWM, and each wheel can be driven independently. Furthermore, there is no backlash because the experimental vehicle has direct drive systems that transmit power directly without a reduction gear. Direct drive systems make it easier for the actual torque to track command value and also makes it possible to obtain information on the reaction force from the road surface from each IWM. Besides,

TABLE I
Physical parameters of the experimental vehicle.

| Item | Value |
|---|---|
| Vehicle mass $M$ | $854\,\mathrm{kg}$ |
| Inertia of the vehicle $J$ | $617\,\mathrm{kg\,m^2}$ |
| Tread $d$ | $1.3\,\mathrm{m}$ |
| Wheelbase | $1.72\,\mathrm{m}$ |
| Distance between the Center of Mass and front wheel | $1.01\,\mathrm{m}$ |
| Distance between the Center of Mass and rear wheel | $0.70\,\mathrm{m}$ |
| Inertia of front wheel $J_{\omega\mathrm{f}}$ | $1.24\,\mathrm{kg\,m^2}$ |
| Inertia of rear wheel $J_{\omega\mathrm{r}}$ | $1.26\,\mathrm{kg\,m^2}$ |
| Wheel radius $r$ | $0.302\,\mathrm{m}$ |

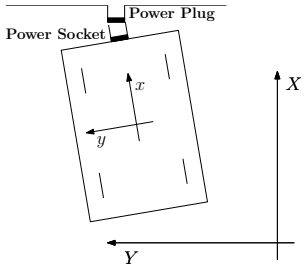


Fig. 3. Schematic diagram of an initial state of a vehicle body with a power plug and a power socket contact with each other, viewed from above.

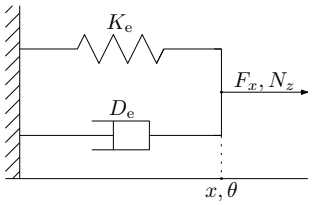


Fig. 4. Model in which the reaction force received by the vehicle from the power plug is expressed as a spring-damper.

the experimental vehicle is equipped with a power plug shown in Fig. 2a and a force/torque sensor shown in Fig. 2b.

### B. Experimental condition

The required tasks can be roughly divided into two steps.

*1) Path planning and path tracking:* The moving path needs to be calculated, and then the vehicle has to move on the route for automatic parking. Path planning and path tracking of non-holonomic vehicles have already been achieved in [8], [9]. In this paper, we assume the situation in which the power plug has contact with the power socket and is about to be inserted. Then we set this state to the initial state.

However, vehicles cannot move in all directions, and the range of fine adjustment is limited because they are non-holonomic systems. Accordingly, we consider the condition in which the position of the power plug and power socket can be matched, but the plug leans slightly, more specifically, about $0.1\,\mathrm{rad}$. Fig. 3 shows the initial state of power plug insertion.

Here, we assume that the vehicle cannot move in the $y$-direction because of non-holonomic constraints. Moreover, the misalignment of the power socket in $y$-direction due to the rotation of the vehicle is ignorable because it is infinitesimal.

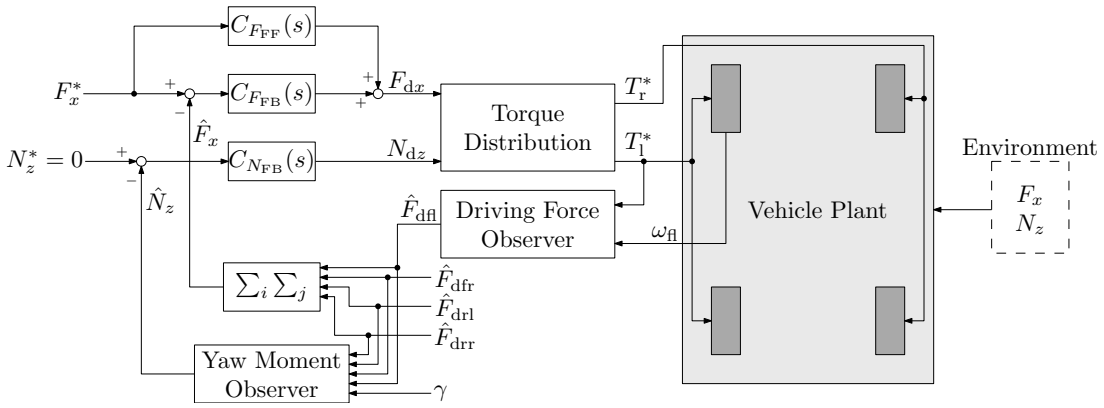


Fig. 5. Block diagram of whole control system.

Because only the rotational motion of the vehicle and the motion in the $x$-direction need to be considered, the steering angle is set as 0, and the vehicle posture is changed only by the difference between the left and right driving forces generated by IWMs. We consider the vehicle motion only on the $x$-$y$ plane and do not deal with the motion in the $z$-axis.

*2) Force control of vehicles:* To insert the power plug without breaking it, it is necessary to perform not only position- and velocity-based control but also force control. The vehicle receives the external force/moment from the environment, i.e., the power plug. Since the environment can be described as a spring-damper model, the reaction force in the x-axis $F_x$ and the reaction moment round the z-axis $N_z$ can be written as

$$F_x = K_{\mathrm{e}_F} x + D_{\mathrm{e}_F} \dot{x} \tag{1}$$

$$N_z = K_{\mathrm{e}_N} \theta + D_{\mathrm{e}_N} \gamma, \tag{2}$$

where $x$ is the position of the vehicle, $\theta$ is the yaw angle of the vehicle, $\gamma$ is the derivative of $\theta$ and $K_{\mathrm{e}_F}, D_{\mathrm{e}_F}, K_{\mathrm{e}_N}, D_{\mathrm{e}_N}$ are the constants.

## III. Force control for power plug insertion control

In this section, we consider the task of inserting a power plug as a force control problem and describe how to apply it to EVs.

### A. Block diagram of the reaction force controller

It is necessary to equalize the angle between the power plug and the power socket and apply an appropriate force to insert the power plug into the power socket without breaking it. This can be achieved by considering a servo system in which the external moment is regulated to 0, and the external force in the traveling direction is regulated to a constant value. It is because the power plug can be described as a spring-damper property in both the traveling direction and the yaw direction of the vehicle.

Fig. 5 shows the block diagram of the whole control system in the proposed method. Since controlled objects are the reaction force and the reaction moment, the reaction force is estimated by the driving force observer (DFO) [18] and the reaction moment is estimated by the yaw-moment observer (YMO) [19], and then they are fed back. The torque input to each IWM is calculated from the action force and the action moment by the torque distribution law.

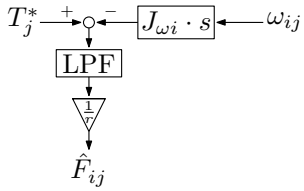


Fig. 6. Driving force observer which estimate the driving force from the torque command and the angular velocity of the wheel.

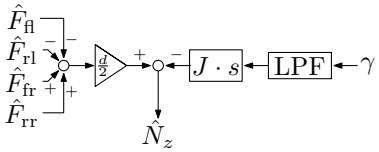


Fig. 7. Yaw-moment observer which estimate the yaw-moment from the torque command and the angular velocity of the body.

### B. Estimation of the reaction force by DFO

Equation of motion for wheel rotation can be written as

$$J_{\omega i} \dot{\omega}_{ij} = T_{ij}^* - r F_{\mathrm{d}xij}, \tag{3}$$

where $J_\omega$ is the inertia of each wheel, $T^*$ is an input torque to each wheel, $\omega$ is angular velocity of each wheel, $r$ is a radius of wheel and $F_{\mathrm{d}}$ is a driving force of each wheel. Subscript $i \in \{\mathrm{f}, \mathrm{r}\}$ and $j \in \{\mathrm{l}, \mathrm{r}\}$ respectively mean front-rear and left-right.

Therefore, the driving force $\hat{F}_{\mathrm{d}ij}$ can be estimated from the input torque and the angular velocity of the wheel by using the DFO shown in Fig. 6 [18]. Since the driving force of the tire is equal to the reaction force exerted on each wheel by the external force and moment, this DFO can estimate the reaction force.

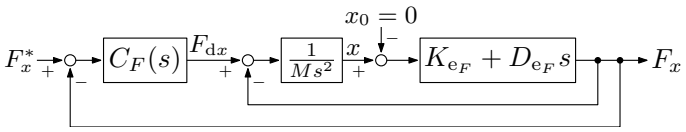


Fig. 8. Block diagram of the feedback controller and the simplified plant for design of the reaction force controller.

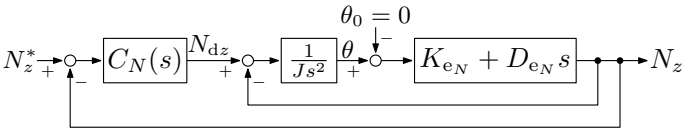


Fig. 9. Block diagram of the feedback controller and the simplified plant for design of the reaction moment controller.

The DFO can estimate the force applied to each wheel from the environment, thereby, the force $F_x$ applied to the vehicle body from the environment can be calculated as

$$\hat{F}_x = \sum_i \sum_j \hat{F}_{\mathrm{d}xij}. \tag{4}$$

Note that the steering angle is 0.

### C. Estimation of the reaction moment by YMO

Equation of motion in the yaw direction of the vehicle can be described as

$$J\dot{\gamma} = \frac{d}{2} \sum_i \left(F_{\mathrm{d}xir} - F_{\mathrm{d}xil}\right) - N_z, \tag{5}$$

where $J$ is the total inertia of the vehicle, $d$ is the distance between left and right wheels (i.e., front and rear tread) and $N_z$ is the reaction moment on the vehicle body.

Therefore, the reaction moment $\hat{N}_z$ can be estimated from estimated driving forces and the yaw rate by using the YMO shown in Fig. 7 [19].

### D. Design of the reaction force/moment feedback controller by the pole placement

Regulating the external moment $N_z$ to 0 achieves the state in which the vehicle and the power plug are oriented in the same direction. It is because contact with the environment generates a reaction moment $N_z$ proportional to the yaw angle of the vehicle body $\theta$, and its derivative, the yaw rate $\gamma$.

Furthermore, since a force in the x-direction is also required when inserting the power plug into the power socket, the feedback controller is designed so that the external force $F_x$ in the x-direction follows the command value $F_x^*$.

Fig. Fig. 8, Fig. 9 respectively shows a block diagram of a nominal plant simplified by an equation of motion $F_{\mathrm{d}x} = M\ddot{x}$ and $N_{\mathrm{d}z} = J\dot{\theta}$. These block diagrams make it easier to calculate the transfer function from the command force in the x-direction $F_x^*$ to the actual reaction force $F_x$. Moreover, the conrollers, $C_{F_{\mathrm{FB}}}(s), C_{N_{\mathrm{FB}}}(s)$ in Fig. 5, are respectively designed as a PID controller with pseudo-differentiation.

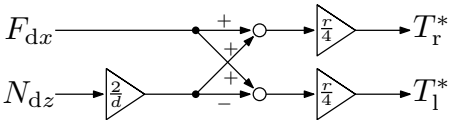


Fig. 10. Block diagram of the torque distribution law to obtain the desired force $F_x$ and moment $N_z$.

The closed-loop transfer function from $F_x^*$ to $F_x$ is fourth order as the equation (7).

$$\frac{F_x}{F_x^*} = \frac{(K_{\mathrm{e}_F} + D_{\mathrm{e}_F} s)(K_{\mathrm{i}_F} + K_{\mathrm{p}_F} s + K_{\mathrm{d}_F} s^2 + \tau_F K_{\mathrm{i}_F} s + \tau_F K_{\mathrm{p}_F} s^2)}{den._F} \tag{6}$$

, where

$$\begin{aligned} den._F = {} & \tau_F M s^4 + \left\{ M + (K_{\mathrm{d}_F} + \tau_F (1 + K_{\mathrm{p}_F})) D_{\mathrm{e}_F} \right\} s^3 \\ & + \left\{ (1 + K_{\mathrm{p}_F} + \tau_F K_{\mathrm{i}_F}) D_{\mathrm{e}_F} + (K_{\mathrm{d}_F} + \tau_F (1 + K_{\mathrm{p}_F})) K_{\mathrm{e}_F} \right\} s^2 \\ & + \left\{ K_{\mathrm{i}_F} D_{\mathrm{e}_F} + (1 + K_{\mathrm{p}_F} + \tau_F K_{\mathrm{i}_F}) K_{\mathrm{e}_F} \right\} s + K_{\mathrm{i}_F} K_{\mathrm{e}_F}. \end{aligned} \tag{7}$$

$$\frac{N_z}{N_z^*} = \frac{(K_{\mathrm{e}_N} + D_{\mathrm{e}_N} s)(K_{\mathrm{i}_N} + K_{\mathrm{p}_N} s + K_{\mathrm{d}_N} s^2 + \tau K_{\mathrm{i}_N} s + \tau K_{\mathrm{p}_N} s^2)}{den._N} \tag{8}$$

$$\tag{9}$$

, where

$$den._N = \tau J s^4 + \left\{ J + (K_{\mathrm{d}_N} + \tau (1 + K_{\mathrm{p}_N})) D_{\mathrm{e}_N} \right\} s^3 \tag{10}$$

$$+ \left\{ (1 + K_{\mathrm{p}_N} + \tau K_{\mathrm{i}_N}) D_{\mathrm{e}_N} + (K_{\mathrm{d}_N} + \tau (1 + K_{\mathrm{p}_N})) K_{\mathrm{e}_N} \right\} s^2 \tag{11}$$

$$+ \left\{ K_{\mathrm{i}_N} D_{\mathrm{e}_N} + (1 + K_{\mathrm{p}_N} + \tau K_{\mathrm{i}_N}) K_{\mathrm{e}_N} \right\} s + K_{\mathrm{i}_N} K_{\mathrm{e}_N}. \tag{12}$$

The poles are placed quadruply here. $K_{\mathrm{e}_F}$ is set to $1 \times 10^4$ and $D_{\mathrm{e}_F}$ is set to $2 \times 10^3$. When the angular frequency of the pole exceeds about $8\,\mathrm{rad\,s^{-1}}$, the proportional gain $K_{\mathrm{p}_F}$ becomes a negative value. Accordingly, the pole is placed below this frequency. Furthermore, we note that the pole does not exceed the frequency of the zero point.

Similarly, the closed-loop transfer function from $N_z^*$ to $N_z$ is also fourth order as the equation (12). The poles are placed quadruply here. Here, $K_{\mathrm{e}_N}$ is set to $3 \times 10^2$ and $D_{\mathrm{e}_F}$ is set to $6 \times 10^1$ When the angular frequency of the pole exceeds about $8\,\mathrm{rad\,s^{-1}}$, the proportional gain $K_{\mathrm{p}_N}$ becomes a negative value. Accordingly, the pole is placed below this frequency. Furthermore, we note that the pole does not exceed the frequency of the zero point.

### E. Design of the reaction force feedforward controller

Considering Fig. 8, the transfer function from $F_{\mathrm{d}x}$ to $F_x$ is described as

$$\frac{F_x}{F_{\mathrm{d}x}} = \frac{D_{\mathrm{e}_F} s + K_{\mathrm{e}_F}}{Ms^2 + D_{\mathrm{e}_F} s + K_{\mathrm{e}_F}}. \tag{13}$$

Therefore, $F_{F_{\mathrm{FF}}}$ is designed as an inversed plant as follows,

$$C_{F_{\mathrm{FF}}}(s) = \frac{Ms^2 + D_{\mathrm{e}_F} s + K_{\mathrm{e}_F}}{D_{\mathrm{e}_F} s + K_{\mathrm{e}_F}} \cdot \frac{\omega_{\mathrm{FF}}}{s + \omega_{\mathrm{FF}}}. \tag{14}$$

Low pass filter is added to make the $C_{F_{\mathrm{FF}}}$ proper controller.

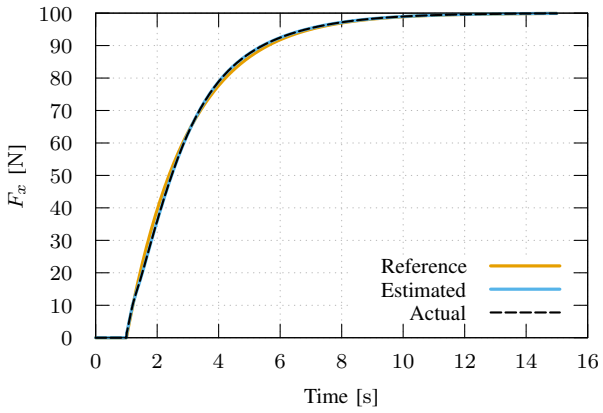


(a) Reaction force.

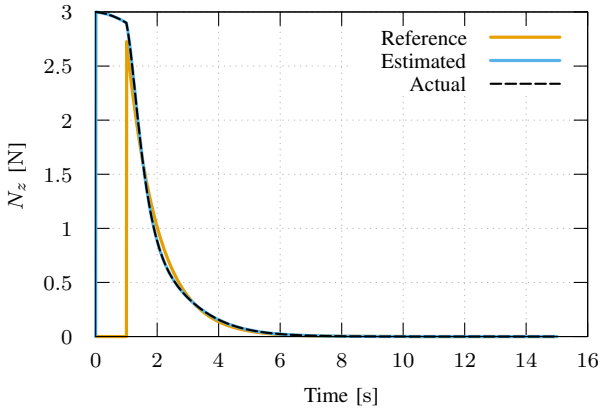


(b) Reaction moment.

Fig. 11. Simulation results. Only estimation is conducted before 1 s and control is started at 1 s.

### F. Distribution law of input torque

With only force constraints, there remains a degree of freedom in torque distribution. Therefore, we add a constraint that the same torque is input to the front and rear IWMs, i.e.,

$$\forall j \in \{\mathrm{l}, \mathrm{r}\}, \quad F_{\mathrm{f}j} = F_{\mathrm{r}j} = \frac{F_j}{2}. \tag{15}$$

Then, the following torque distribution law,

$$\begin{bmatrix} F_{\mathrm{d}x} \\ N_{\mathrm{d}z} \end{bmatrix} = \begin{bmatrix} 1 & 1 \\ -d/2 & d/2 \end{bmatrix} \begin{bmatrix} F_{\mathrm{dl}} \\ F_{\mathrm{dr}} \end{bmatrix} \tag{16}$$

$$\therefore \begin{bmatrix} F_{\mathrm{dl}} \\ F_{\mathrm{dr}} \end{bmatrix} = \begin{bmatrix} 1/2 & -1/d \\ 1/2 & 1/d \end{bmatrix} \begin{bmatrix} F_{\mathrm{d}x} \\ N_{\mathrm{d}z} \end{bmatrix}, \tag{17}$$

can be obtained. Fig. 10 shows the block diagram of the torque distribution law.

## IV. Results

### A. Simulation Results

Simulation to validate the proposed method is conducted in Matlab Simulink. The vehicle can be considered as a differential wheeled vehicle since the input torque of the front and rear IWMs is equal. Hence, a differential wheeled system is used as a plant in the simulation.

Small reaction force at the moment when the power socket contacts the power plug and slow changes of the reaction force are desirable from a safety point of view. Accordingly, the final target value of the reaction force $F_x^*$ is 100 N, and the force gradually approaches to the final value from 0 N exponentially with a time constant of 2 s. Then, the final target value of the external moment $N_z^*$ is set to 0, the reaction moment gradually approaches to the final value from the initial value exponentially with a time constant 1 s. This command value ensures safety because the external moment is controlled more slowly than when inputting step command. Note that the time constant of the reaction moment command is shorter than that of the reaction force so that the power plug is not broken by applying great force before the vehicle angle converges.

The angular frequency of both PID controllers are placed at $5\,\mathrm{rad\,s^{-1}}$ at this simulation. The cutoff angular frequency of LPF is set to $30\,\mathrm{rad\,s^{-1}}$.

Simulation results are shown in Fig. 11a and Fig. 11b Note that only estimation is performed until $t = 1$ s since differential values diverge immediately after the start of the simulation. Furthermore, the servo system functions well, i.e., the force and moment follow the target values without a steady deviation or overshoot.

### B. Experimental Results

Our proposed method is also verified in the hardware experiment with the experimental setup shown in Fig. 1. The target value of the reaction force is set to 100 N, and that of the reaction moment is set to 0 N m. The angular frequency of the reaction force feedback controller $C_{F_{\mathrm{FB}}}$ is placed at $3\,\mathrm{rad\,s^{-1}}$, and that of the reaction moment feedback controller $C_{F_{\mathrm{FB}}}$ is placed at $3.5\,\mathrm{rad\,s^{-1}}$ in the experiment.

Fig. 12(a) shows the timed reaction force and its estimates. The estimates are slightly noisy because of signal line noise produced by power inverter, but the smoothed estimates follow the reference value well. Furthermore, the proposed method estimates the actual reaction force accurately.

Fig. 12(b) shows the timed reaction moment. The estimation of the reaction moment does not work well, and the estimates could not be used for control. Therefore, estimates are not plotted in Fig. 12(b), and measured value is used for control. The proposed method can make the reaction moment close to zero, but the steady deviation remains. These are probably because the reaction moment is too small to be observed by the information of wheel encoders and is affected by road friction.

## V. Conclusion

In this paper, we propose a control method for automatic power plug insertion by controlling the reaction moment to zero with the reaction force/moment estimation with DFO and YMO. Feedback and Feedforward controllers are designed based on transfer functions.

The simulation of the proposed method shows that estimates of the reaction force and reaction moment are in good agreement with actual values and that the torque distribution law can

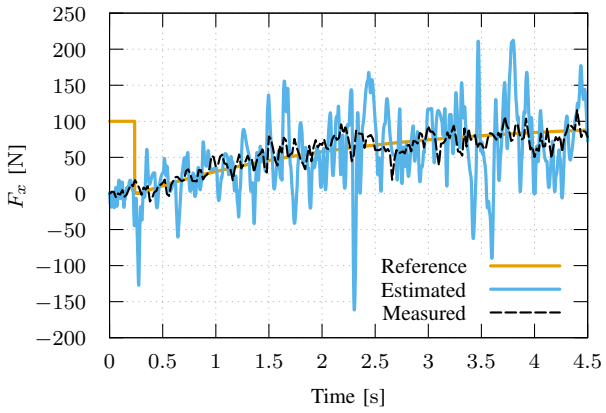


(a) Reaction force.

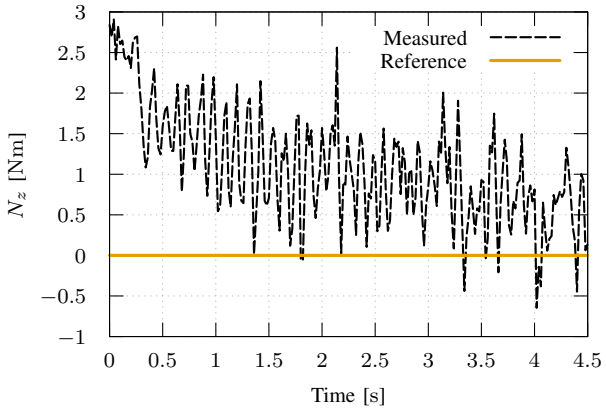


(b) Reaction moment.

Fig. 12. Experimental results.

make them follow target values appropriately. Furthermore, the experimental results confirm that the proposed method can achieve automatic power plug insertion without breaking it.

It remains a challenge for future research to propose a method for automatic power plug insertion in onboard motor type EVs with electric power steering (EPS). It is because IWM type EVs are inevitably more expensive than onboard motor type EVs due to the increased number of motors. Future works also include reduction of the power plug misalignment by considering dynamics under the non-holonomic constraints without neglecting motion in the $y$-direction. The control of vehicle motion in the $z$-axis should also be worked on future research. Steady deviation of the reaction moment seen in the experimental results is expected to be reduced by considering non-holonomic constraints with EPS.

## VI. Acknowledgment

This work was partly supported by JSPS KAKENHI Grant Number JP18H03768, Industrial Technology Research Grant Program from New Energy and Industrial Technology Development Organization (NEDO) of Japan (number 05A48701d) and MEXT KAKENHI Grant Numbers JP22246057, JP26249061.

## References

[1] Y. Hori, "Future vehicle driven by electricity and control - Research on four-wheel-motored "UOT Electric March II"," *IEEE Transactions on Industrial Electronics*, vol. 51, no. 5, pp. 954–962, 2004.

[2] M. Galvani, F. Biral, B. M. Nguyen, and H. Fujimoto, "Four wheel optimal autonomous steering for improving safety in emergency collision avoidance manoeuvres," in *2014 IEEE 13th International Workshop on Advanced Motion Control (AMC)*. IEEE, mar 2014, pp. 362–367.

[3] S. Yamada, T. Beauduin, H. Fujimoto, T. Kanou, and E. Katsuyama, "Model-based longitudinal vibration suppression control for electric vehicles with geared in-wheel motors," in *2017 IEEE International Conference on Advanced Intelligent Mechatronics (AIM)*. IEEE, jul 2017, pp. 517–522.

[4] V.-D. Doan, H. Fujimoto, T. Koseki, T. Yasuda, H. Kishi, and T. Fujita, "Iterative Dynamic Programming for Optimal Control Problem with Isoperimetric Constraint and Its Application to Optimal Eco-driving Control of Electric Vehicle," *IEEJ Journal of Industry Applications*, vol. 7, no. 1, pp. 80–92, 2018.

[5] H. Fujimoto, T. Takeuchi, K. Hanajiri, K. Hata, T. Imuta, M. Sato, D. Gunji, and G. Guidi, "Development of Second Generation Wireless In-Wheel Motor with Dynamic Wireless Power Transfer," *The 31st International Electric Vehicle Symposium & Exhibition and International Electric Vehicle Technology Conference 2018*, 2018.

[6] T. Tajima and H. Tanaka, "Study of 450-kW Ultra Power Dynamic Charging System," in *WCX World Congress Experience*. SAE International, apr 2018.

[7] G. Lovison, T. Imura, H. Fujimoto, and Y. Hori, "Secondary-side-only Phase-shifting Voltage Stabilization Control with a Single Converter for WPT Systems with Constant Power Load," *IEEJ Journal of Industry Applications*, vol. 8, no. 1, pp. 66–74, 2019.

[8] M. Sobue, H. Fujimoto, and Y. Hori, "RRT-Based Path Planning Considering Initial and Final Pose for Nonholonomic Wheeled Robots," in *SAMCON*, 2019.

[9] M. Hashimoto, N. Suizu, and F. Oba, "Path Tracking Control Method of a Modular Omnidirectional Vehicle," *Nihon Kikai Gakkai Ronbunshu, C Hen/Transactions of the Japan Society of Mechanical Engineers, Part C*, vol. 66, no. 648, pp. 2713–2720, 2000.

[10] T. Enmei, H. Fujimoto, and Y. Hori, "Proposal of impedance control for electric vehicles with wheel resolver - Application to hand assisted parking and position adjustment -," *IECON Proceedings (Industrial Electronics Conference)*, pp. 6435–6440, 2016.

[11] K. Alexis, C. Huerzeler, and R. Siegwart, "Hybrid modeling and control of a coaxial unmanned rotorcraft interacting with its environment through contact," *Proceedings - IEEE International Conference on Robotics and Automation*, pp. 5417–5424, 2013.

[12] T. Tomić, C. Ott, and S. Haddadin, "External wrench estimation, collision detection, and reflex reaction for flying robots," *IEEE Transactions on Robotics*, vol. 33, no. 6, pp. 1467–1482, 2017.

[13] M. Haruna, I. Kim, K. Fukushima, S. Sofuku, T. Nakaoji, J. Takaki, Y. Saruta, N. Kawaguchi, Y. Horiuchi, and Y. Ezaki, "Force control technology of segment mirror exchange robot for Thirty Meter Telescope (TMT)," *Ground-based and Airborne Telescopes VI*, vol. 9906, no. July 2016, p. 99062Z, 2016.

[14] A. Briod, P. Kornatowski, A. Klaptocz, A. Garnier, M. Pagnamenta, J. C. Zufferey, and D. Floreano, "Contact-based navigation for an autonomous flying robot," *IEEE International Conference on Intelligent Robots and Systems*, pp. 3987–3992, 2013.

[15] N. Hogan, "Impedance Control: An Approach to Manipulation," in *1984 American Control Conference*. IEEE, jul 1984, pp. 304–313.

[16] M. H. Raibert and J. J. Craig, "Hybrid Position/Force Control of Manipulators," *Journal of Dynamic Systems, Measurement, and Control*, vol. 103, no. 2, pp. 126–133, jun 1981.

[17] M. Morisawa and K. Ohnishi, "Dynamic Hybrid Control," *Science And Technology*, vol. 11, no. 8715798, pp. 381–386, 2004.

[18] M. Yoshimura and H. Fujimoto, "Driving torque control method for electric vehicle with in-wheel motors," *IEEJ Transactions on Industry Applications*, vol. 131, no. 5, pp. 721–728, 2011.

[19] N. Ando and H. Fujimoto, "Yaw-rate control for electric vehicle with active front/rear steering and driving/braking force distribution of rear wheels," in *2010 11th IEEE International Workshop on Advanced Motion Control (AMC)*. IEEE, mar 2010, pp. 726–731.